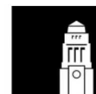


This is a repository copy of *Tunable hot-carrier photodetection beyond the bandgap spectral limit*.

White Rose Research Online URL for this paper:
http://eprints.whiterose.ac.uk/78934/

Version: Supplemental Material

**Article:**

Lao, Y-F, Perera, AGU, Li, LH orcid.org/0000-0003-4998-7259 et al. (3 more authors) (2014) Tunable hot-carrier photodetection beyond the bandgap spectral limit. Nature Photonics, 8 (5). pp. 412-418. ISSN 1749-4885

https://doi.org/10.1038/nphoton.2014.80

**Reuse**
Items deposited in White Rose Research Online are protected by copyright, with all rights reserved unless indicated otherwise. They may be downloaded and/or printed for private study, or other acts as permitted by national copyright laws. The publisher or other rights holders may allow further reproduction and re-use of the full text version. This is indicated by the licence information on the White Rose Research Online record for the item.

**Takedown**
If you consider content in White Rose Research Online to be in breach of UK law, please notify us by emailing eprints@whiterose.ac.uk including the URL of the record and the reason for the withdrawal request.

eprints@whiterose.ac.uk
https://eprints.whiterose.ac.uk/

# Supplementary Information

## Tunable hot-carrier photodetection beyond the band-gap spectral limit

Yan-Feng Lao[1], A. G. Unil Perera[1], L. H. Li[2], S. P. Khanna[2], E. H. Linfield[2], and H. C. Liu[3]

[1] Department of Physics and Astronomy, Georgia State University, Atlanta, GA 30303, USA
[2] School of Electronic and Electrical Engineering, University of Leeds, Leeds LS2 9JT, United Kingdom
[3] Key Laboratory of Artificial Structures and Quantum Control, Department of Physics, Shanghai Jiao Tong University, Shanghai 200240, China

# I Supplementary Methods

Prior to the photoresponse measurements, the dark current-voltage-temperature (I-V-T) characteristics were evaluated (See the Methods section of the paper). This allows determination of the value of the activation energy ($\Delta$). A typical experimental apparatus for photoresponse measurements is shown in Fig. S1a, where a Perkin-Elmer system 2000 Fourier transform infrared (FTIR) spectrometer is used. Light from the FTIR spectrometer is guided into the dewar by the plane and concave mirrors, and concentrated on the detector sample by a Winston cone, which is placed in front of the sample. The short-wavelength portion of the FTIR light (pump optical source) excites holes in the injector which are then injected into the absorber under a negative bias. The long-wavelength portion of the FTIR light acts as a probe to the very long-wavelength infrared (VLWIR) photoresponse. Such a pump-probe measurement was also demonstrated by the experiment using separate pump and probe optical sources, as shown in Fig. S1b. Figure 3a of the paper shows a schematic diagram of this experimental system. Here, a long-pass filter is inserted into the optical path to block the short-wavelength portion of the FTIR light. By using a semi-insulating double-side polished GaAs wafer as a beamsplitter, the light from the optical excitation source (pump) is mixed with the FTIR light (the long-wavelength portion) incident on the detector sample.

To calibrate the spectral responsivity, a Si composite bolometer, which has a constant sensitivity over the entire wavelength range, was measured. The experimental arrangement for measuring the sample and bolometer (mounted in the same dewar) uses the identical optical path with the same optical components. The spectral responsivity is thus obtained using the following expression:

$$\mathcal{R} = C \cdot \left[\mathcal{I}_d \,/\, \mathcal{I}_b\right] \tag{1}$$

where $\mathcal{I}_d$ and $\mathcal{I}_b$ are the intensities of the signal from the detector sample and bolometer, re-

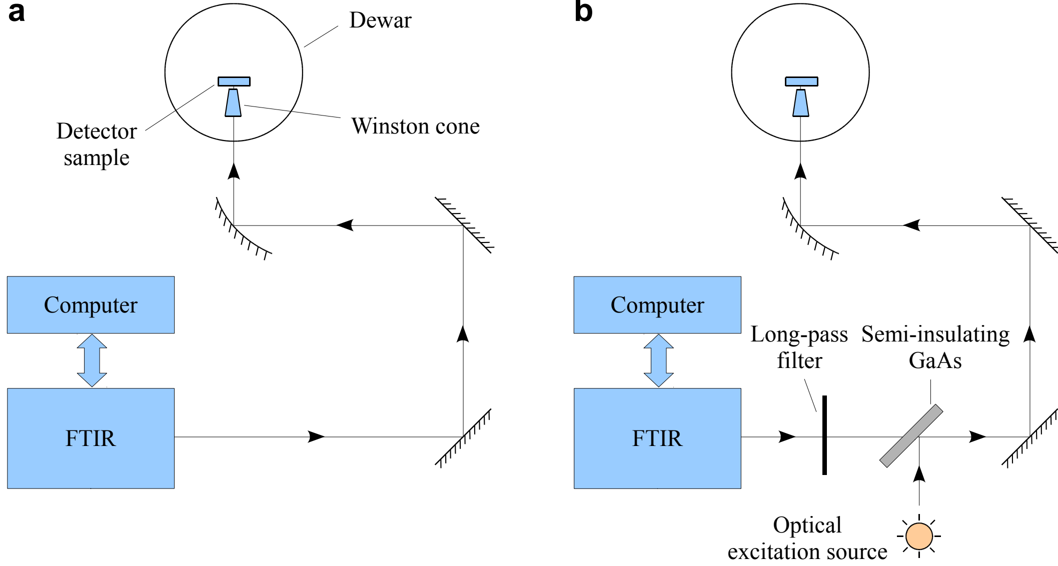


Figure S1: **a,** Experimental apparatus for photoresponse measurements. The short-wavelength portion of the FTIR light acts as a pump to inject hot holes, whereas the long-wavelength portion probes the VLWIR response. **b,** Photoresponse measurements with separate pump and probe optical sources. A long-pass filter is used to block the short-wavelength portion of the FTIR light. An external optical excitation source is used as a pump, which is guided into the optical path by a GaAs beamsplitter.

spectively. $C$ is a calibrating factor independent of the wavelength, which takes into account the sensitivity of the bolometer, differences between the parameters of measuring the detector and bolometer (e.g., the active detection area and the preamplifier gain), and the resistances of the detector and load resistor. The load resistor is used as a voltage divider, with a fixed resistance of $7 \times 10^7$ Ohm for all the measurements.

# II Supplementary Discussion

## 1. Confirming the VLWIR response

The photoresponse threshold of previously reported internal-photoemission heterojunction detectors [1, 2, 3] has agreed very well with a detection limit determined by $\lambda_c = hc/\Delta$. Observing a response beyond 4 $\mu$m in the present sample ($\Delta = 0.32$ eV) is, therefore, surprising. It is essential to confirm that the observed VLWIR response is not a result of experimental artifacts. In the paper, evidence is presented to verify the VLWIR response. This includes: (1) the escape-cone model simulation, (2) measuring hole distribution peaks at applied biases when the VLWIR response rises, and (3) measuring the tunable VLWIR response through varying the pump optical source (using filters/an external optical excitation source). In addition to these measurements, the experiment using an external optical excitation source and a GaAs wafer (beamsplitter) further validated the VLWIR response. The spectral response is plotted in Fig. S2. Since GaAs lies in the optical path

(see Fig. S1b), it absorbs light. Therefore, the response should contain the absorption features of GaAs. As expected, dips in the $15-30$ $\mu$m wavelength range of the response spectra are confirmed as being due to multiple phonon absorptions in GaAs, by comparing with the transmission spectrum (inset). This confirms that the response signal in the VLWIR range is due to the FTIR light.

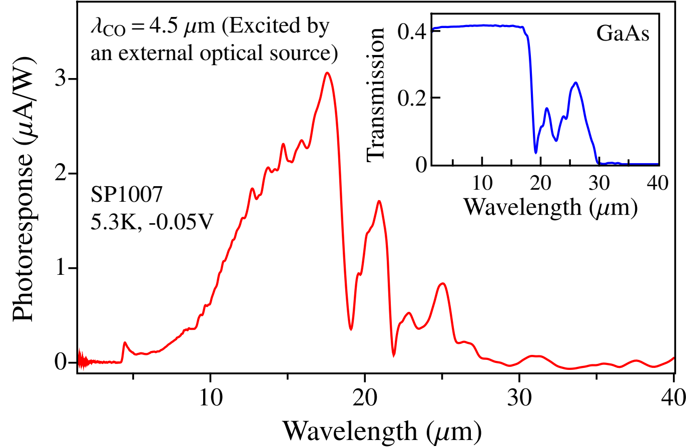


Figure S2: Photoresponse of sample SP1007 measured using the experimental apparatus of Fig. S1b, in which the cut-on wavelength ($\lambda_{CO}$) of the long-pass filter is 4.5 $\mu$m. Inset: transmission spectrum of GaAs (with an incident angle of 45°). As GaAs lies in the optical path, its phonon absorption features appear on the response spectrum.

## 2. Activation energy based on I-V-T data

The activation energy can be obtained from the $R_0A$-T behavior, where $R_0$ is the zero-bias differential resistance, and $A$ is the active area. The $R_0A$ values were calculated by using experimental I-V-T data, and plotted as a function of temperature on a logarithmic scale, i.e., an Arrhenius plot, as shown in Fig. S3. A previously reported symmetrical flat-barrier GaAs/$Al_{0.57}Ga_{0.43}As$ detector (sample SP3) [4] is also shown for comparison. Fits to the Arrhenius plots gave activation energies ($E_A$) of 0.30 eV and 0.40 eV for samples SP3 and SP1007, respectively. The values of $E_A$ can be considered as those of $\Delta$, [5] which agree well with the designed values of 0.32 eV and 0.42 eV, corresponding to the $p$-type GaAs/$Al_{0.57}Ga_{0.43}As$ and GaAs/$Al_{0.75}Ga_{0.25}As$ junctions, respectively. [1] For the samples used in the paper, we cannot actually measure the activation energy associated with the $p$-type GaAs (absorber)/$Al_{0.57}Ga_{0.43}As$ (constant barrier) junction; instead, the highest barrier height (associated with the GaAs/$Al_{0.75}Ga_{0.25}As$ graded barrier junction) was obtained (see Fig. S3). As such, we refer to the designed value ($\Delta = 0.32$ eV) as the conventional threshold energy for operation under a reverse bias.

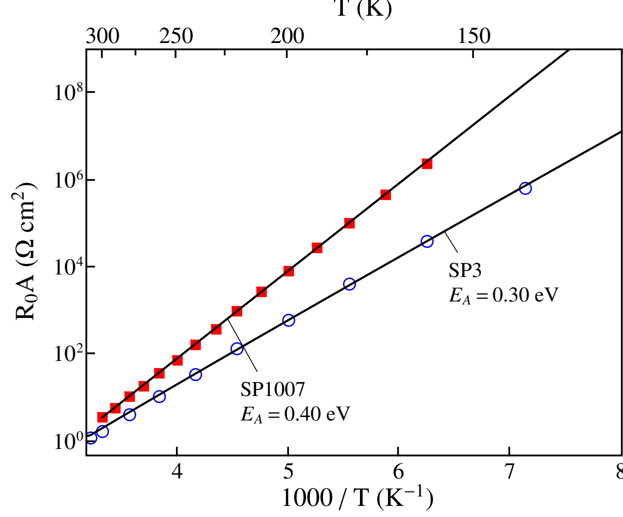


Figure S3: The Arrhenius plots of $R_0A$ against $1000/T$, to determine the activation energies ($E_A$). Also shown is a previously reported [4] symmetrical flat-barrier GaAs/$Al_{0.57}Ga_{0.43}As$ detector (SP3).

## 3. The escape-cone model

Carrier emission across the emitter/barrier heterointerface is typically described as an internal photoemission process, for which the emission probability can be evaluated by an escape-cone model. The principle is to calculate the number of carriers which are capable of escaping over a potential barrier by having a normal (to the interface) momentum greater than that of the barrier. These carriers occupy energy states on a spherical Fermi cap in $\boldsymbol{k}$ space. [6] This model can be used to extract the threshold energy of photoemission, [6, 7] and also to simulate the spectral response of heterojunction photodetectors. [8, 9] Since this model has been described in the literature, [6, 7, 8] it will not be repeated here. For example, Ref. [8] presents the escape-cone model for doped heterostructures. To calculate the spectral response, the total quantum efficiency should be evaluated, which essentially divides into two parts: the escape efficiency (probability), and the absorption efficiency. The latter needs separating into two absorption mechanisms for the $p$-type GaAs absorber, i.e., intra- and inter-valence-band optical transitions. According to our calculations, intra-valence-band transitions lead to good fits to the experimental photoresponse in the VLWIR range. In contrast, inter-valence-band transitions mostly dominate in the wavelength range below 10 $\mu$m. [10]

## 4. Bias-dependent VLWIR response

Representative response spectra at different applied biases are shown in Fig. S4a. The general profile between $5-50$ $\mu$m agrees with the escape-cone model, as shown in the manuscript. However, there are two response peaks at $\sim 25.3$ and 35.6 $\mu$m (or 395 and 281 cm$^{-1}$ in wavenumber) which becomes apparent at higher negative bias (up to $-0.3$ V). The 25.3-$\mu$m peak becomes strong for

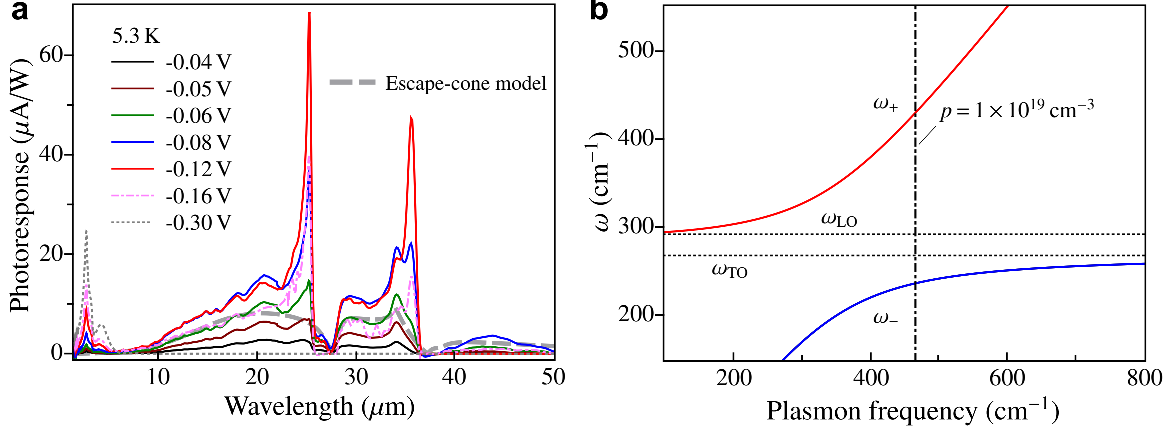


Figure S4: **a,** Bias-dependent photoresponse of SP1007. The general spectral profile agrees with the escape-cone model. Two sharp peaks are seen at $\sim 25.3$ and $35.6$ $\mu$m (or 395 and 281 cm$^{-1}$ in wavenumber) that disagree with the model. These are observed at negative biases higher than $-0.06$ V. **b,** Calculated plasmon-phonon coupling modes [11] ($\omega_+$ and $\omega_-$). The calculation takes into account damping. [12] The two modes at $p = 1 \times 10^{19}$ roughly match with the positions of the two sharp peaks shown in **a**.

bias greater than $-0.06$ V, and the 35.6-$\mu$m peak rises when the bias is greater than $-0.08$ V. In the very long-wavelength range, the absorption in the GaAs absorber is dominated by intra-band free-carrier transitions and phonon absorptions. It has been shown that, when the plasmon frequency is comparable to the longitudinal optical (LO) phonon frequency, [11] strong coupling between the plasmon and LO modes is expected, giving rise to two coupling modes, $\omega_+$ and $\omega_-$, as shown in Fig. S4b. It was found that the two sharp response peaks in Fig. S4a are close to $\omega_+$ and $\omega_-$ for $p = 1 \times 10^{19}$ cm$^{-3}$ (the doping concentration in the GaAs absorber), which are 430 cm$^{-1}$ (or 23 $\mu$m) and 236 cm$^{-1}$ (or 42 $\mu$m), respectively. Notice that the coupling modes were calculated based on equilibrium distribution without the hot-hole effect. Upon the injection of hot holes, part of the cold hole distribution acquires energy from hot holes and is excited into higher energy states. In terms of our experimental conditions, the total concentration of holes in the absorber should be close to the original doping concentration (i.e., $1 \times 10^{19}$ cm$^{-3}$). However, their distribution could vary greatly from that without hot-hole injection. This means that the calculation shown in Fig. S4b may not be an actual representation of the coupling. In spite of the hot-hole effect, comparison between the two sharp response peaks and the coupling modes implies the important role of the phonon-plasmon coupling in affecting the response. We feel more detailed studies are needed to understand this fully, and this is out of the scope of the present work. Despite this, the observed VLWIR response is experimentally confirmed (see Sec. II.1.), and its general spectral profile is in agreement with the prediction of the escape-cone model.

## 5. Photoresponse of the symmetrical flat-barrier detector

It is found that having a barrier offset ($\delta E_v$; see Fig. 1 (c) of the paper) is essential to obtain the VLWIR response. This assertion is experimentally demonstrated by comparing the photoresponse of samples with (SP1005 – 1007) and without (LH1002) $\delta E_v$, as shown in Fig. 1e in the paper. The values of $\delta E_v$ are 0.10 eV and 0 eV for SP1005 – 1007 and LH1002, respectively. The VLWIR response of three samples SP1005 – 1007 all have similar spectral profiles. As expected, however, sample LH1002 does not show any VLWIR response at all. We have carefully checked different bias voltages between -1 V and 1 V in LH1002, which cover the entire electric field range used for measuring SP1005 – SP1007 when the VLWIR response occurs. Except for the gradual redshift of the response threshold with increasing bias (owing to barrier lowering [1]), no response in the VLWIR range can be observed.

It may be noted that high-energy hot holes can be injected into the absorber of sample LH1002 by applying a higher bias. This might be expected to increase the hot-cold hole interactions and lead to hole distribution peaks being observed. However, as shown in Fig. S5, a differential photocurrent peak is only seen at 0 V. From comparisons with the differential photocurrents of SP1007 and hot-carrier spectroscopy [13, 14, 15], this is unlikely to be a result of hot-cold hole interactions. In hot-carrier spectroscopy, a carrier distribution peak is typically observed when the potential barrier on the injection side is higher than that in the collection side, and this differs from the operation of LH1002.

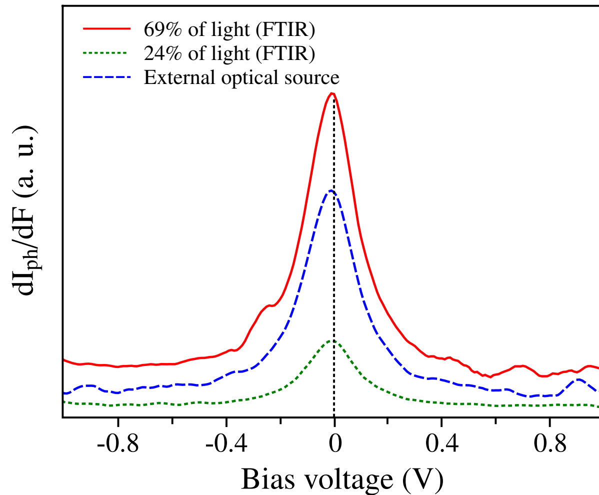


Figure S5: Differential photocurrents ($dI_{ph}/dF$) for the symmetrical flat-barrier sample LH1002, measured using different optical excitation sources. A peak is only observed at 0 V.

## 6. VLWIR response at different temperatures

The VLWIR response spectra at different temperatures are shown in Fig. S6. It can be seen that responsivities at short- and long-wavelength (i.e., $< 4$ and $> 4$ $\mu$m, respectively) display the

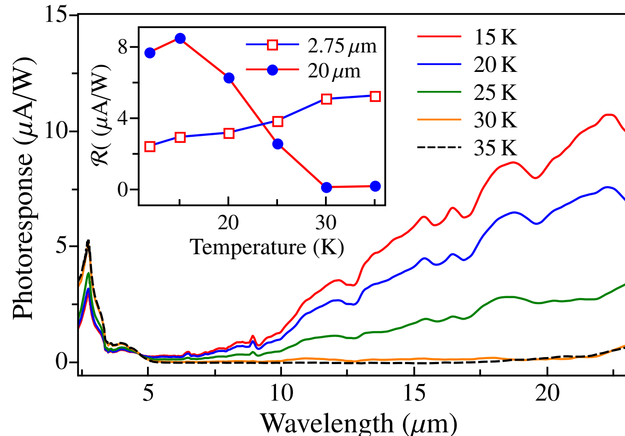


Figure S6: Photoresponse of SP1007 at different temperatures (at $-0.1$ V). Inset: the values of responsivity as a function of temperature at 2.75 and 20 $\mu$m.

opposite temperature dependences (see inset of Fig. S6). The VLWIR ($> 4$ $\mu$m) response decreases with temperature and can be observed only up to 30 K. At 35 K, it is flat, nearly at the spectral noise level. This could be due to the variation of the dominant scattering with temperature. With increasing temperature, carrier-carrier scattering can be affected by other processes such as carrier-ionized dopant scattering. The reduction in the carrier-carrier scattering rate will then decrease the efficiency of energy transfer from hot carriers to cold carriers. Consequently, the cold carriers are less likely to be excited which in turn decreases the VLWIR response. In contrast, an increase in the concentration of cold holes at higher temperatures contributes to the increased response for wavelengths $< 4$ $\mu$m. This explains the increase in the short-wavelength response with increased temperature. It should be noted, though, that the sample can only respond up to 4 $\mu$m for temperature above 30 K. This is the "normal" response (in accordance with $\lambda_c = hc/\Delta$). However, this short-wavelength response can be even observed at room temperature. [16] All of these experimental results are consistent with our proposed hot-hole mechanism. Further optimized structures, e.g., using quantum structures as the absorber, may improve the operating temperature, as quantum structures posses a longer carrier lifetime than bulk semiconductors.

## III Supplementary References


[1] Lao, Y.-F. & Perera, A. G. U. Temperature-dependent internal photoemission probe for band parameters. *Phys. Rev. B* **86**, 195315 (2012).

[2] Matsik, S. G. *et al.* Cutoff tailorability of heterojunction terahertz detectors. *Appl. Phys. Lett.* **82**, 139–141 (2003).

[3] Rinzan, M. B. M. *et al.* AlGaAs emitter/GaAs barrier terahertz detector with a 2.3 THz threshold. *Appl. Phys. Lett.* **86**, 071112 (2005).

[4] Jayaweera, P. V. V. *et al.* Uncooled infrared detectors for $3-5$ $\mu$m and beyond. *Appl. Phys. Lett.* **93**, 021105 (2008).

[5] Batey, J. & Wright, S. L. Energy band alignment in GaAs:(Al,Ga)As heterostructures: The dependence on alloy composition. *J. Appl. Phys.* **59**, 200–209 (1986).

[6] Williams, R. *Injection phenomena*. Semiconductors and Semimetals (Academic Press, New York, 1970).

[7] Goodman, A. M. Photoemission of electrons from $n$-type degenerate silicon into silicon dioxide. *Phys. Rev.* **152**, 785–787 (1966).

[8] Rinzan, M., Matsik, S. & Perera, A. Quantum mechanical effects in internal photoemission THz detectors. *Infrared Phys.& Technol.* **50**, 199 – 205 (2007).

[9] Esaev, D. G., Rinzan, M. B. M., Matsik, S. G. & Perera, A. G. U. Design and optimization of GaAs/AlGaAs heterojunction infrared detectors. *J. Appl. Phys.* **96**, 4588–4597 (2004).

[10] Lao, Y.-F. & Perera, A. G. U. Dielectric function model for $p$-type semiconductor inter-valence band transitions. *J. Appl. Phys.* **109**, 103528 (2011).

[11] Olson, C. G. & Lynch, D. W. Longitudinal-optical-phonon-plasmon coupling in GaAs. *Phys. Rev.* **177**, 1231–1234 (1969).

[12] Giehler, M. & Jahne, E. Effect of damping on the plasmon-phonon coupling in CdS and GaP. *physica status solidi (b)* **73**, 503–516 (1976).

[13] Brill, B. & Heiblum, M. Electron heating in GaAs due to electron-electron interactions. *Phys. Rev. B* **49**, 14762–14765 (1994).

[14] Hayes, J. R., Levi, A. F. J. & Wiegmann, W. Hot-electron sectroscopy of GaAs. *Phys. Rev. Lett.* **54**, 1570–1572 (1985).

[15] Levi, A. F. J., Hayes, J. R., Platzman, P. M. & Wiegmann, W. Injected-hot-electron transport in GaAs. *Phys. Rev. Lett.* **55**, 2071–2073 (1985).

[16] Pitigala, P. K. D. D. P. *et al.* Photovoltaic infrared detection with $p$-type graded barrier heterostructures. *J. Appl. Phys.* **111**, 084505 (2012).